

## BeppoSAX OBSERVATIONS OF THE X-RAY PULSAR MAXI J1409–619 IN LOW STATE: DISCOVERY OF CYCLOTRON RESONANCE FEATURES

MAURO ORLANDINI<sup>1</sup>, FILIPPO FRONTERA<sup>1,2</sup>, NICOLA MASETTI<sup>1</sup>, VITO SGUERA<sup>1</sup>, AND LARA SIDOLI<sup>3</sup>

<sup>1</sup> INAF/Istituto di Astrofisica Spaziale e Fisica Cosmica (IASF) Bologna, via Gobetti 101, 40129 Bologna, Italy

<sup>2</sup> Dipartimento di Fisica, Università degli Studi di Ferrara, via Saragat 1, 44122 Ferrara, Italy

<sup>3</sup> INAF/Istituto di Astrofisica Spaziale e Fisica Cosmica (IASF) Milano, via Bassini 15, 20133 Milano, Italy

Received 2011 September 13; accepted 2012 January 19; published 2012 March 12

### ABSTRACT

The transient 500 s X-ray pulsar MAXI J1409–619 was discovered by the slit cameras aboard *Monitor of All-sky X-ray Image* (MAXI) on 2010 October 17, and soon after accurately localized by *Swift*. We found that the source position was serendipitously observed in 2000 during *BeppoSAX* observations of the Galactic plane. Two sources are clearly detected in the Medium-Energy Concentrator Spectrometer (MECS): one is consistent with the position of IGR J14043–6148 and the other one with that of MAXI J1409–619. We report on the analysis of this archival *BeppoSAX*/MECS observation integrated with newly analyzed observation from *ASCA* and a set of high-energy observations obtained from the offset fields of the *BeppoSAX*/PDS instrument. For the ON-source observation, the 1.8–100 keV spectrum is fit by an absorbed power law with a photon index  $\Gamma = 0.87^{+0.29}_{-0.19}$ , corresponding to 2–10 and 15–100 keV unabsorbed fluxes of  $2.7 \times 10^{-12}$  and  $4 \times 10^{-11}$  erg cm<sup>-2</sup> s<sup>-1</sup>, respectively, and a 2–10 keV luminosity of  $7 \times 10^{34}$  erg s<sup>-1</sup> for a 15 kpc distance. For a PDS offset field observation, performed about one year later and showing a 15–100 keV flux of  $7 \times 10^{-11}$  erg cm<sup>-2</sup> s<sup>-1</sup>, we clearly pinpoint three spectral absorption features at 44, 73, and 128 keV, resolved both in the spectral fit and in the Crab ratio. We interpret these not harmonically spaced features as due to cyclotron resonances. The fundamental energy of  $44 \pm 3$  keV corresponds to a magnetic field strength at the neutron star surface of  $3.8 \times 10^{12}(1+z)$  G, where  $z$  is the gravitational redshift. We discuss the nature of the source in the light of its possible counterpart.

**Key words:** stars: individual (IGR J14043-6148, MAXI J1409–619) – X-rays: binaries

*Online-only material:* color figures

### 1. INTRODUCTION

On 2010 October 17 Yamaoka et al. (2010b) reported on an outburst from a new source, named MAXI J1409–619, revealed by the Gas Slit Camera (GSC; Mihara et al. 2002) of the *Monitor of All-sky X-ray Image* (MAXI; Matsuoka et al. 2009) experiment aboard the International Space Station. The 4–10 keV flux decreased from its initial value of  $\sim 40$  mCrab on October 17 to  $\sim 30$  mCrab on the following day.

On October 20 *Swift* (Gehrels et al. 2004) began a target of opportunity observation of the MAXI J1409–619 error circle (0.2 radius). Kennea et al. (2010b) used the X-Ray Telescope (XRT; Burrows et al. 2005) to pinpoint the position of the new source with an estimated 90% confidence level uncertainty of 1.9 and coordinates R.A. (J2000): 14<sup>h</sup>08<sup>m</sup>02<sup>s</sup>.56, decl. (J2000):  $-61^{\circ}59'00''.3$ . Its spectrum is fit by an absorbed power law, with photon index  $\Gamma = -0.5^{+0.1}_{-0.6}$ . A follow-up XRT observation on November 30 found the source  $\sim 7$  times brighter than on October 20, with an average 0.3–10 keV flux of  $7 \times 10^{-10}$  erg cm<sup>-2</sup> s<sup>-1</sup> (Kennea et al. 2010a). Only in this latter observation was a  $\sim 500$  s pulsation detected, with a 42% sinusoidal rms modulation. The source has been detected since October 18 also in the 15–50 keV energy band by the *Swift* Burst Alert Telescope (BAT; Barthelmy et al. 2005) at the level of  $\sim 30$  mCrab (Kennea et al. 2011).

Neither cataloged radio nor X-ray sources were present in the *Swift* error circle, while a Two Micron All Sky Survey (2MASS) IR star, the likely IR counterpart of the X-ray transient, lies 2.1 from the XRT position (Kennea et al. 2010b).

The source was also observed on October 22 by the Proportional Counter Array (PCA; Jahoda et al. 1996) aboard *RXTE*

(Bradt et al. 1993). The X-ray spectrum shows a strong 6.5 keV iron line (E.W. 200 eV) and a continuum modeled by reflection or partially covering absorption (Yamaoka et al. 2010a). The 2–10 keV flux was about  $10^{-10}$  erg cm<sup>-2</sup> s<sup>-1</sup> and was strongly variable on timescales of hundreds of seconds. An observation performed on December 4 found MAXI J1409–619 at a flux level 6–7 times higher than the October observation (Yamamoto et al. 2010) and confirmed the 500 s pulse period observed by *Swift*.

From observations performed on December 2 and 3 by the GLAST Burst Monitor (GBM; Meegan et al. 2007) aboard the *Fermi* satellite, the presence of a 500 s double-peaked pulsating signal was confirmed (Camero-Arranz et al. 2010).

Following the MAXI J1409–619 localization by *Swift*, we searched for *BeppoSAX* (Boella et al. 1997a) archival observations with the transient position within the Narrow Field Instruments (NFIs) field of view (FoV). We found that an observation performed in the framework of a Galactic plane survey contained the MAXI J1409–619 position (Sguera et al. 2010).

In this paper, we report on the spectral analysis of this *BeppoSAX* observation, integrated with high-energy data obtained from the offset fields of the PDS (Frontera et al. 1997) instrument. We further present the analysis of a newly analyzed *ASCA* observation performed during a Galactic plane survey.

### 2. OBSERVATIONS

#### 2.1. BeppoSAX/PDS Observations

We searched our *BeppoSAX* archive for observations covering the MAXI J1409–619 position. From our local archive we are able to extract not only products from the NFI nominal pointings

**Table 1**  
List of PDS Pointings Covering the MAXI J1409–619 Error Box

Seq	OPn	Date	Duration (ks)	Source Name	Distance ( $^{\circ}$ )	R.A. (J2000)	Decl. (J2000)	Type	PDS Rate (15–100 keV counts s $^{-1}$ )	S/N
1	08317	2000 Jan 29	42	Gal Plane Sur 2	19.6	211.3474	–61.88437	ON	$0.247 \pm 0.069$	3.6
2	10480	2001 Jan 7	220	Circinus Galaxy	27.3	212.8952	–61.80250	MOFF	$0.450 \pm 0.032$	14.1
3	08386	2000 Feb 7	52	Gal Plane Sur 16	49.5	210.2841	–61.83828	ON	$0.086 \pm 0.049$	1.7
4	01652	1997 Feb 23	90	Alpha Cen	53.6	213.5273	–62.53019	POFF	$0.086 \pm 0.052$	1.6
5	08484	2000 Feb 19	47	Gal Plane Sur 23	70.0	213.5936	–61.09281	POFF	$0.144 \pm 0.072$	2.0

**Notes.** The “Source Name” refers, in case of offset fields, to the nominal ON pointing. The distance listed in Column 6 refers to the angular distance of the PDS pointing from the MAXI J1409–619 position.

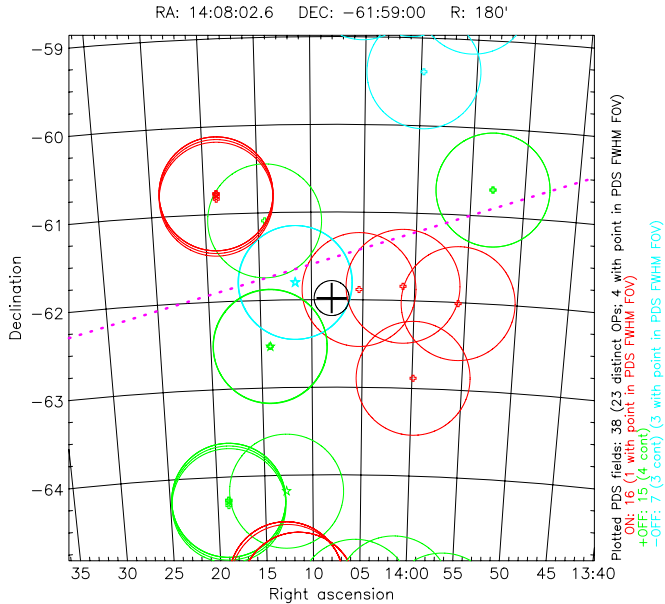


**Figure 1.** Region centered on the MAXI J1409–619 position (the small black circle) with the PDS pointings: ON pointings (red), POFF pointings (green), and MOFF pointings (cyan). The PDS FoV is  $1^{\circ}3$  (FWHM). Note the two PDS observations (one ON and one MOFF) fully covering the source position, and three (one ON and two POFF) partially covering the position (with the term “partially” we intend that the source is beyond the collimator FWHM but before its FWZI). The bold dotted line corresponds to the Galactic plane.

(A color version of this figure is available in the online journal.)

(also available from ASDC—the ASI Scientific Data Center<sup>4</sup>) but also net spectra from the PDS offset fields.

Indeed, because of the rocking technique used to derive the PDS background, two positions offset by  $3^{\circ}5$  with respect to the NFI direction were alternatively observed every 96 s. For fields free of sources, we expect that differences between the count spectra in the “plus OFF” (hereafter POFF) and “minus OFF” (hereafter MOFF) positions will be consistent with zero. If, on the other hand, a contaminating source is present in one of the two offset fields, then the spectral difference corresponds to a net, background-subtracted PDS spectrum of the offset field.

We found three sets of observations containing the MAXI J1409–619 position in their FoVs. In Figure 1, we show a finding chart centered on the MAXI J1409–619 position and showing both the ON-source and OFF-source pointings (the PDS FoV is  $1^{\circ}3$  FWHM). In Table 1, we detail the whole set of *BeppoSAX* observations used in our analysis. All errors are given at the 90% confidence level for a single parameter.

### 2.1.1. ON-source Observations (OP08317 and OP08386)

The first ON-source *BeppoSAX* pointing with MAXI J1409–619 in the NFI FoV was performed on 2000 January 29 within a program aimed at performing a systematic study of part of the Galactic plane (OP08317—Galactic Plane Survey Field 02). Another ON-source observation (OP08386—Galactic Plane Survey Field 16) was performed a week later. This observation partially overlaps the OP08317 field (see Figure 1).

The Galactic plane Field 02 net exposures of the two imaging instruments Low-Energy Concentrator Spectrometer (LECS; 0.1–10 keV; 37' FoV; Parmar et al. 1997) and Medium-Energy Concentrator Spectrometer (MECS; 1.8–10 keV; 56' FoV; Boella et al. 1997b) are 6812 and 22,060 s, respectively. The difference is due to the constraint that the LECS can be operated only when in the Earth shadow. Good data were selected when the instrument configurations were nominal, and with an elevation angle above the Earth limb  $>4^{\circ}$ .

A mosaic of the two, partially overlapping, ON-source OP08317 and OP08386 MECS images is shown in Figure 2, where two relatively bright sources are clearly present (see Table 2). Source 2 position is consistent with MAXI J1409–619, while the source 1 position is consistent with the X-ray source IGR J14043–6148 (Bird et al. 2010). The third detection (source 3) corresponds to extended low-energy emission observed in the LECS image and may be associated with a radio source at approximately the same position (Cohen & Green 2001). The uncertainty in the MECS positions is 30" (Perri & Capalbi 2002).

We extracted LECS and MECS data from a  $4'$  (30 pixel) radius circular region centered on the MAXI J1409–619 position. Concerning LECS data, there are not enough counts to allow a spectral reconstruction. On the other hand, we are able to extract a 1.8–10 keV MECS spectrum that we rebinned to a minimum of 30 counts bin $^{-1}$  to allow the use of  $\chi^2$  statistics. We used a response matrix appropriate for the off-axis position of the source. Because the position of MAXI J1409–619 is close to the Galactic plane, we checked for possible contamination from the Galactic ridge emission. To this end, from the MECS image we extracted background spectra from two source-free regions, offset by about the same angle as the source (to take into account vignetting), and with the same extraction radii. These backgrounds are consistent with the mean background used routinely for MECS observations. For this reason the mean background was used in the spectral analysis.

Given that the PDS is not an imaging instrument, before performing joint MECS/PDS spectral fits it is necessary to address the problem of determining whether the high-energy

<sup>4</sup> <http://www.asdc.asi.it/bepposax>

**Table 2**  
Sources Detected in the MECS Field for OP08317

Source	Rate <sup>a</sup>		Pixel		R.A.	Decl.	S/N	Counterpart
	(2–10 keV)		<i>x</i>	<i>y</i>				
1	45.5	3.6	373.2	317.1	14 04 31.3	−61 47 10.8	12.6	IGR J14043–6148
2	10.6	1.3	188.2	233.2	14 08 00.4	−61 58 24.1	8.15	MAXI J1409–619
3	3.77	0.79	293.9	250.1	14 06 00.5	−61 56 09.6	4.77	

**Note.** <sup>a</sup> In units of  $10^{-3}$  counts  $s^{-1}$ .

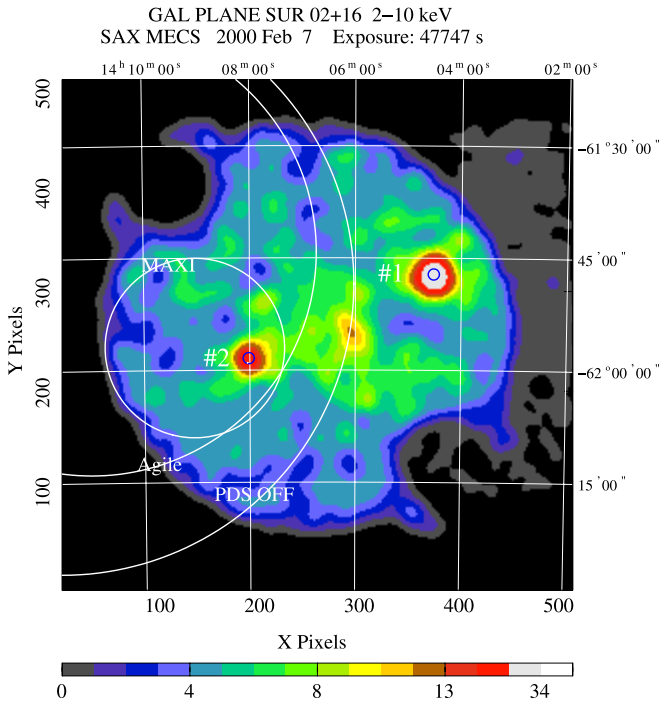


**Figure 2.** 2–10 keV MECS image of a mosaic of the two, partially overlapping, ON-source *BeppoSAX* observations OP08317 and OP08386, smoothed with a Gaussian filter with a  $\sigma$  of  $24''$ . Two sources are clearly detected. The one present in the MAXI J1409–619 error box is listed as source 2 in Table 2. The two “cutouts” are due to the removal of the calibration source events. (A color version of this figure is available in the online journal.)

emission observed by the PDS is due to MAXI J1409–619 or to the *INTEGRAL* source. Bear in mind that, in computing fluxes, it is necessary to take into account the triangular angular response of the PDS collimators (see Figure 2 in Frontera et al. 2007).

First, we analyzed the ON-source OP08386 MECS observation that contains IGR J14043–6148 (detected at  $>15\sigma$ ) but not MAXI J1409–619. For this observation we have only a marginal PDS detection (see Table 1), therefore it seems plausible to associate the high-energy emission observed in the OP08317 observation with MAXI J1409–619. To further confirm this association, we verified that the PDS spectrum extrapolated at lower energies is consistent with the MAXI J1409–619 MECS spectrum.

In Figure 3, we show the joint MECS/PDS 1.8–100 keV MAXI J1409–619 count rate spectrum, together with its power-law best fit (normalized  $\chi^2_\nu$  of 0.18 for 15 degrees of freedom, dof). It is characterized by a hard spectrum, with power-law photon index  $0.87^{+0.29}_{-0.19}$ ,  $N_H = 2.8^{+3.4}_{-2.2} \times 10^{22} \text{ cm}^{-2}$  (consistent with galactic absorption, Dickey & Lockman 1990) and unabsorbed 2–10 and 15–100 keV fluxes of  $2.7 \times 10^{-12}$  and  $4 \times 10^{-11} \text{ erg cm}^{-2} \text{ s}^{-1}$ , respectively.

### 2.1.2. MOFF Offset Field Observation (OP10480)

From Figure 1 we can see that we have three sets of PDS offset observations covering the MAXI J1409–619 position. For two of them (OP01652 and OP08484) we do not have sufficient statistics to perform a useful analysis (see the observed count rates in Table 1). On the other hand, for the MOFF offset field of the Circinus Galaxy observation, OP10480, data have enough statistics for a thorough spectral analysis.

First, we checked for the presence of any cataloged X-ray sources in the MOFF observation FoV. The only source present is the *EGRET* (Hartman et al. 1999) source 3EG J1410–6147 that was recently associated with the 50 ms radio pulsar PSR J1410–6132 (O’Brien et al. 2008). No significant X-ray emission has been detected around the *EGRET* source (Doherty et al. 2003); therefore, we associate the PDS detection with MAXI J1409–619.

We started by extracting a 15–100 keV coarser binned PDS spectrum of the MOFF field (assuming as its background the corresponding POFF spectrum). The fit with a power law gives a photon index of  $2.2 \pm 0.3$ , with a normalized  $\chi^2_\nu$  of 1.31 for 11 dof. From the shape of the residuals and from the quite different photon index with respect to the ON-source observation, we suspected the presence of a change of slope in the spectrum between 20 and 30 keV. This break is not detected in the ON-source observation because of its poor statistics. We tried both a broken and a cutoff power law. By fixing the cutoff energy at 25 keV (we were only able to constrain the break/cutoff energy between 20 and 40 keV), a cutoff power-law fit gives a power-law index  $\Gamma = 0.9^{+0.4}_{-0.3}$ , with a normalized  $\chi^2_\nu$  of 1.06 for 11 dof. While from a statistical point of view the two fits are equivalent (an *F*-test gives a 36% probability of chance improvement (PCI) of the  $\chi^2$ —see Appendix A for the discussion on the correctness of the use of the *F*-test), the cutoff fit nicely matches the spectral index observed at lower energies. The corresponding 15–100 keV flux, corrected for the triangular response of the collimator, is  $7.0 \times 10^{-11} \text{ erg cm}^{-2} \text{ s}^{-1}$ .

Intrigued by the shape of the residuals, we tried a smaller rebinning factor and a wider (15–200 keV) energy range. We were surprised to find the spectrum shown in Figure 4. Absorption features at  $\sim 40$ ,  $\sim 70$ , and  $\sim 120$  keV are quite evident. We also noted that the points that trail these features at  $\sim 50$ ,  $\sim 90$ , and  $\sim 150$  keV seem to be in agreement with a hard continuum up to 200 keV. To test this hypothesis, we performed a fit to the data below 30 keV together with these trailing points. No cutoff (the break energy is not constrained) or broken power-law (the two photon indices are equal) model is able to fit the data, while a power law with photon index  $1.0 \pm 0.2$  does ( $\chi^2_\nu = 0.56$  for 20 dof). Therefore, the change of slope in 20–40 keV derived from the analysis of the coarser binned energy spectrum is really due to the presence of the absorption features. The first absorption feature drives the position of the break, while the higher energy ones are spread by the rebinning,

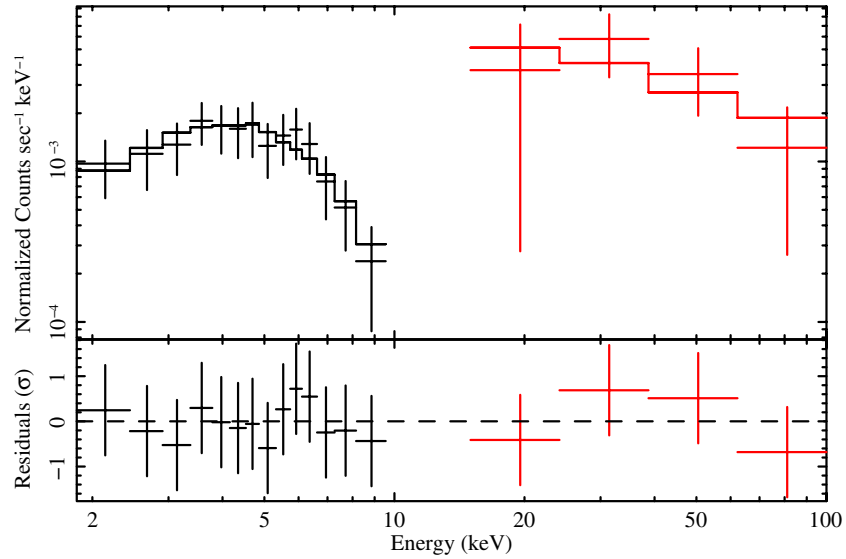


**Figure 3.** 1.8–100 keV joint MECS/PDS count rate spectrum (plus signs) and the power-law best-fit model (histogram) of MAXI J1409–619 in the OP08317 field. The fit residuals are shown in the bottom panel.

(A color version of this figure is available in the online journal.)

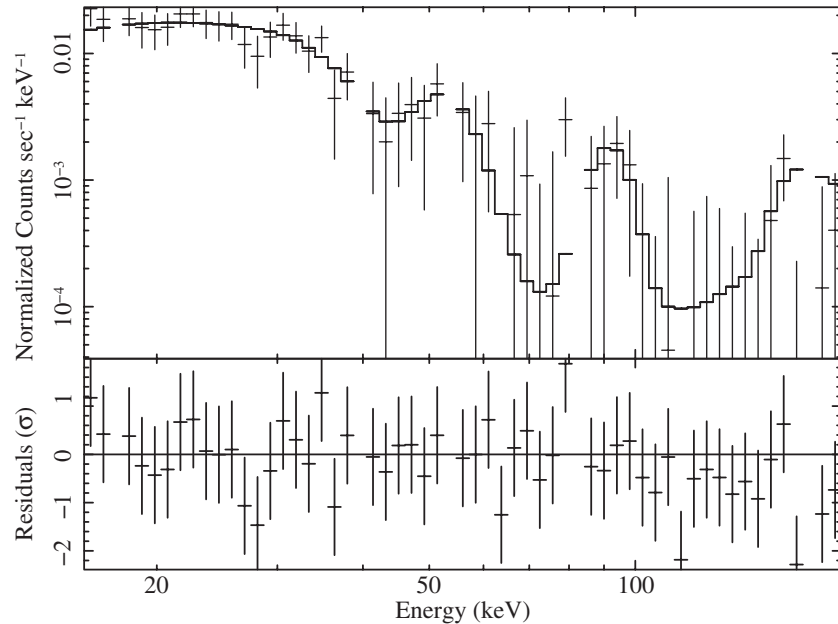


**Figure 4.** 15–200 keV MOFF PDS count rate spectrum (plus signs) and the best-fit power law plus three Gaussians in absorption model (histogram). The fit residuals are shown in the bottom panel. The Gaussian energies are left free and are  $44 \pm 3$ ,  $73^{+4}_{-5}$ , and  $128^{+5}_{-8}$  keV. The line widths were constrained to 4, 4, and 7 keV for the three lines.

resulting in low-count, high-energy bins that are fit by a change of slope.

To further support this interpretation, we performed a joint fit with the MECS spectrum (this analysis is detailed in Appendix B). We find that a cutoff or a broken power-law models are not able to fit this broadband spectrum with the constraint  $\Gamma \sim 0.9$  below 10 keV. This implies that the origin of the change of slope is not due to the presence of a cutoff but to something else, likely absorption features. For these reasons as the continuum we will use a power law with  $\Gamma$  fixed at 0.87, as derived by the analysis on the broadband spectrum of the first observation.

As thoroughly discussed in Appendix A, the assessment of the statistical significance of these absorption features has to be done with great care. Our strategy was to evaluate the significance of

each feature one at a time. We started with a power-law fit in the energy range 15–55 keV, and we obtained an unacceptable  $\chi^2_\nu$  of 1.4 for 25 dof. The inclusion of a Gaussian in absorption (gabs in XSPEC) with centroid energy  $E_{\text{cyc}} = 44 \pm 3$  keV,  $\tau = 16^{+14}_{-7}$ , and width fixed at 4 keV significantly improved the fit ( $\chi^2_\nu$  equal to 0.48 for 23 dof).

Two comments on this measurement are in order: first, the  $\sim 44$  keV line is statistically significant (PCI is  $6 \times 10^{-3}$ ). Second, the difficulties in determining the other line parameters (the line width had to be fixed, while the line normalization is affected by large errors) are due to the fact that the lines are seen as “holes” in the continuum: we have not enough statistics to clearly reconstruct the line profile. The line width is therefore computed from the “hole” width, while for the line depth we



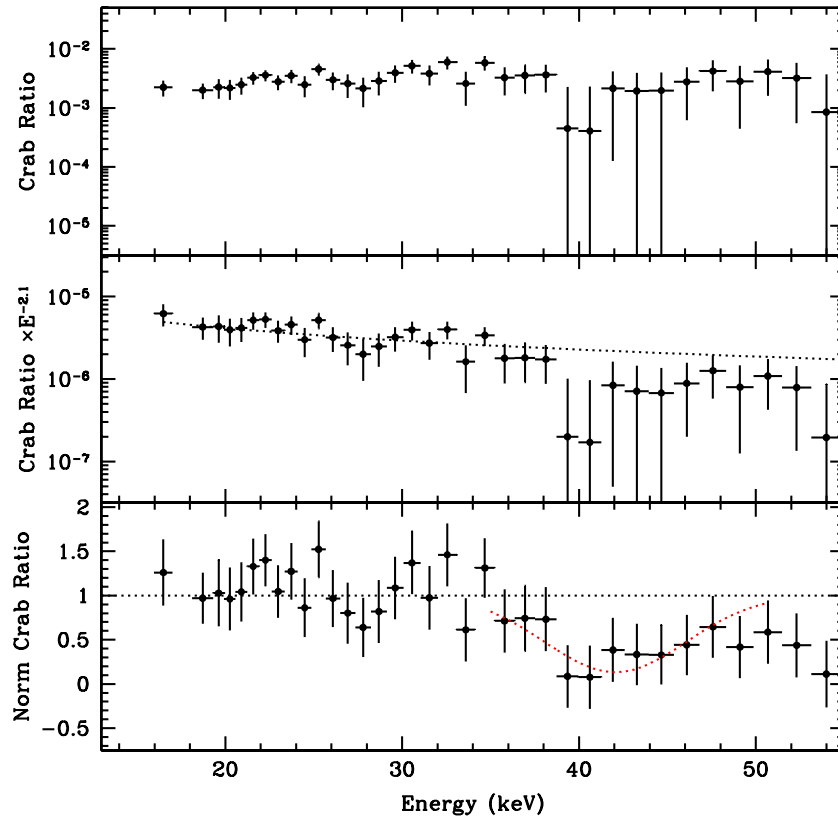


**Figure 5.** Top: ratio between MAXI J1409–619 MOFF and Crab count rate spectra. Middle: the MAXI J1409–619/Crab ratio multiplied by  $E^{-2.1}$ , the functional form of the Crab spectrum. The dotted line corresponds to the best-fit power-law continuum. Bottom: ratio between the former expression and the best-fit power-law continuum, together with a Gaussian fit to the  $\sim 43$  keV CRF. The statistical assessment of the CRF has been evaluated with a run test, finding that we can reject the line being random at the 99% confidence level (see the text and Appendix A for details).

(A color version of this figure is available in the online journal.)

can infer only an upper limit (this will be more evident for the lines at higher energies).

Following our detection strategy, we performed a second fit on the 15–80 keV energy range. The fit with only one Gaussian in absorption was not acceptable:  $\chi^2_\nu$  was 3.6 for 32 dof. By adding another Gaussian in absorption we obtained a significantly better fit, with  $\chi^2_\nu$  of 0.48 for 30 dof (PCI is  $2 \times 10^{-7}$ ). The second line parameters are  $E_{\text{cyc}} = 73^{+4}_{-5}$  keV,  $\tau = 91^{+\infty}_{-42}$ , while the line width was fixed at 7 keV. Note how the two line energies are not in a harmonic ratio.

Then we extended the energy range to the whole 15–200 keV band. Again the fit with two lines was not acceptable ( $\chi^2_\nu$  of 4.5 for 46 dof), so we added another absorption line, the width of which was fixed at 7 keV. The fit significantly improved ( $\chi^2_\nu$  of 0.58 for 44 dof, PCI of  $10^{-10}$ ), with the best fit  $E_{\text{cyc}} = 128^{+5}_{-8}$  keV.  $\tau$  was not constrained (this was not a surprise because, as discussed above, we have no signal in the “hole,” and therefore we are not able to put a limit to the line normalization).

Finally, we constrained the line energies to be in a harmonic ratio. In this case we obtain a  $\chi^2_\nu$  of 1.22 for 46 dof. The best-fit parameters of the fundamental<sup>5</sup> were  $E_{\text{cyc}} = 41 \pm 1$  keV,  $\tau = 11^{+9}_{-7}$ . All the line widths were fixed, as in the previous case with the line energies left free, but we were not able to constrain the (1:2) and (1:3) line normalizations.

In order to verify that the observed features were not of instrumental origin, and at the same time to better characterize the cyclotron resonance features (hereafter CRFs), we performed a normalized Crab ratio analysis (Orlandini 2004) on the MOFF spectrum, as we successfully employed for the detection of CRFs in numerous X-ray pulsars (see, e.g., Orlandini et al. 1998). As it is evident from the top panel of Figure 5, the ratio between the MAXI J1409–619 and the Crab count rate spectra shows a “hole” in the 38–44 keV range due to the fundamental CRF. To enhance the feature, we multiplied the MAXI J1409–619/Crab ratio by the functional form of the Crab spectrum, i.e., a simple power law with photon index equal to 2.1. The result is shown in the second panel of Figure 5. Finally, in the lower panel, we show the ratio between the previous function and the MAXI J1409–619 best-fit continuum power-law model, together with a Gaussian fit to the fundamental CRF. The Gaussian width was fixed at 4 keV, while the Gaussian centroid energy is  $43^{+2}_{-1}$  keV. Please note that this value is a lower limit because it does not take into account the intrinsic energy resolution of the PDS instrument.

In order to give a quantitative evaluation of the CRF in the normalized Crab ratio we performed a run test (see detailed discussion in Appendix A). Up to  $\sim 34$  keV the residuals are consistent with random fluctuations ( $N_+ = 12$ ;  $N_- = 9$ ;  $N_r = 13$ ; consistent with random fluctuation at the 84%). On the other hand, in the 34–50 keV band we see a clear structure in the residuals. In this case from a run test with  $N_+ = 2$ ,  $N_- = 14$ ,  $N_r = 2$  we can reject the null hypothesis of randomness at the 99% confidence level.

<sup>5</sup> Hereafter we will indicate the fundamental resonance as (1:1), meaning with this the ordinal number of the resonance with respect to the fundamental. With this notation the first harmonic will be indicated as (1:2), the third (1:3), and so on.

## 2.2. ASCA Observation

The region around MAXI J1409–619 was observed by *ASCA* on 1998 March 2 for a net exposure time of about 18 ks. The source is clearly detected and its spectrum is confirmed to be quite hard, with a best-fit power-law photon index  $\Gamma = 0.1^{+0.8}_{-0.6}$  and an unabsorbed 1–10 keV flux of  $3 \times 10^{-12}$  erg cm<sup>-2</sup> s<sup>-1</sup>. The absorption in the direction of the source is not well constrained by the fit, with an upper limit of  $3 \times 10^{22}$  cm<sup>-2</sup>, consistent with the *Swift* and *BeppoSAX*/MECS results.

## 3. A VERY RED(DENED) COUNTERPART FOR MAXI J1409–619

As stressed by Kennea et al. (2010b), a NIR source belonging to the 2MASS catalog (Skrutskie et al. 2006) is found within 2'1 of the MAXI J1409–619 position as determined by the XRT. According to that catalog, this source (labeled as 2MASS J14080271–6159020) has NIR magnitudes  $J = 15.874 \pm 0.086$ ,  $H = 13.620 \pm 0.022$ , and  $K = 12.560 \pm 0.021$ . No cataloged optical counterpart is present at the position of this NIR source, and inspection of the DSS-II-Red digitized archival plates<sup>6</sup> does not show any evident optical object at that location. Following Monet et al. (2003) we can thus place a conservative upper limit,  $R > 20$ , to the  $R$ -band magnitude of the optical counterpart of this source. The above magnitudes thus indicate that this is an extremely red object.

Indeed, assuming the Milky Way extinction law (Cardelli et al. 1989), we find that the NIR color indices of this source are consistent with those of a late O/early B-type star (Wegner 1994) with a reddening of  $A_V \approx 20$  mag. This, using the formula of Predehl & Schmitt (1995), implies a column density of  $N_H \sim 3.6 \times 10^{22}$  cm<sup>-2</sup>, which is consistent with that inferred from the *Swift* and *BeppoSAX* spectral analysis results. This large extinction is also supported by the non-detection of the optical counterpart of the source. All this points to a likely high-mass X-ray binary (HMXB) nature of this source, hosting a heavily absorbed early-type star, similar to several cases of *INTEGRAL* hard X-ray sources identified as HMXBs at optical and/or NIR wavelengths (see, e.g., Masetti et al. 2010).

Assuming then  $A_V \approx 20$  mag along the MAXI J1409–619 line of sight and a B0 spectral type for the companion star in this system, we can infer its distance, depending on the luminosity class (main sequence, giant or supergiant) of the star. Using the tabulated absolute magnitudes for this type of star (Lang 1992) we find, for these three cases, respective distances of  $\sim 4.6$ ,  $\sim 7.9$ , and  $\sim 14.5$  kpc. Given that the large absorption found along the line of sight of this source at both NIR and X-ray wavelengths is consistent with the Galactic one, we consider it most likely that the correct distance is the largest one. Thus, MAXI J1409–619 is quite likely located on the far side of the Galaxy, i.e., in the farthest parts of the Sagittarius–Carina arm, and its mass donor star is likely an early-type supergiant.

## 4. DISCUSSION

We found five sets of observations containing the position of MAXI J1409–619 in our *BeppoSAX*/PDS archive, performed in 1997, 2000, and 2001, and one in the *ASCA* archive (1998 March). In all our observations the source was in a low state, with 15–100 keV fluxes in the range  $\sim 2$ –8 mCrab, and no spectral variability during the observations. For comparison, an integrated exposure (over 5 years) of 2.4 ms by

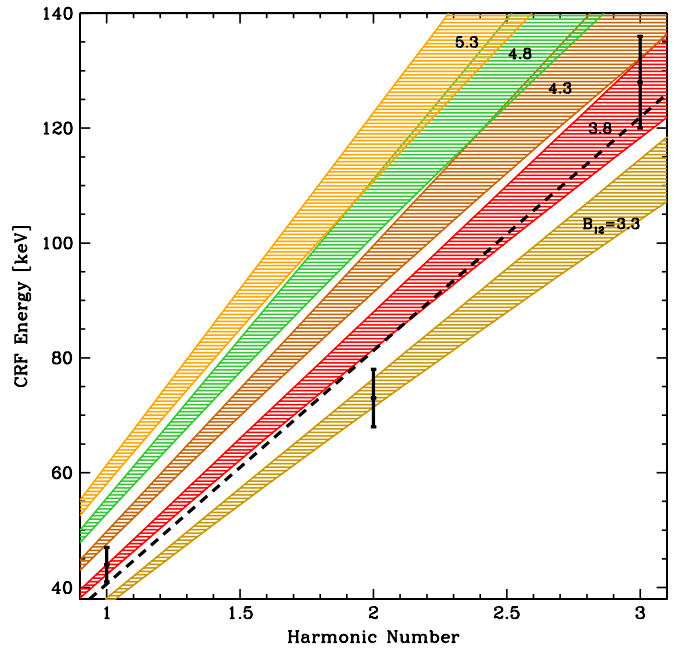


**Figure 6.** Harmonicity of the MAXI J1409–619 CRF line energies. The dashed black line corresponds to a linear fit (that is,  $E_n = n E_1$ ) to the data, while the colored strips take into account relativistic effects, as detailed by Equation (1). Each strip corresponds to a fixed value of the magnetic field strength  $B = B_{12} \times 10^{12}$  G and to a range 0.0001–1 for  $\sin^2 \theta$ , where  $\theta$  is the angle between the photon direction and that of the magnetic field. While  $E_1$  and  $E_3$  are consistent with  $B_{12} \sim 3.8$ ,  $E_2$  is consistent with a magnetic field about 20% lower.

(A color version of this figure is available in the online journal.)

*INTEGRAL*/IBIS provides  $2\sigma$  upper limits on the persistent quiescent emission of 0.2 and 0.4 mCrab in the 20–40 and 40–100 keV energy bands, respectively (Sguera et al. 2010). When assuming the source fluxes in outburst as measured by *Swift* (Kennea et al. 2010b, 2011) and *RXTE* (Yamamoto et al. 2010), from our low-state measurement we can infer a dynamic range of 400 in 15–50 keV and of 300 in 2–10 keV.

The discovery of CRFs in the low-state spectrum of MAXI J1409–619, together with its  $\sim 500$  s pulsations, unambiguously identifies the source as an accreting X-ray binary pulsar. Only a few sources show multiple CRFs, and only two show resonances above the (1:2). Three CRFs were observed during the 2004–2005 outburst of the X-ray pulsar V0332+53 (Coburn et al. 2005; Kreykenbohm et al. 2005; Tsygankov et al. 2006), and five (possibly six) CRFs were discovered in the spectrum of 4U 0115+63 during its 1999 giant outburst (Santangelo et al. 1999; Heindl et al. 1999; Ferrigno et al. 2009). In both cases, deviations from a pure harmonic ratio among the CRFs were observed and were explained in terms of departures from a classical dipolar structure of the magnetic field in the line-forming region (Nishimura 2005, 2008).

The magnetic field strength at the neutron star surface corresponding to  $E_{\text{cyc}} = 44$  keV is  $3.8 \times 10^{12}(1+z)$  G (Canuto & Ventura 1977), where  $z$ , the gravitational redshift, for a typical neutron star of mass  $1.4 M_\odot$  and radius 10 km, is about 0.3. When left as free parameters in the fit, we found that the best-fit CRF line energies do not follow the harmonic relation  $E_n = n E_1$ . A slight non-harmonicity is expected when relativistic effects are taken into account (see, e.g., Meszaros 1992):

<sup>6</sup> <http://archive.eso.org/dss/dss>

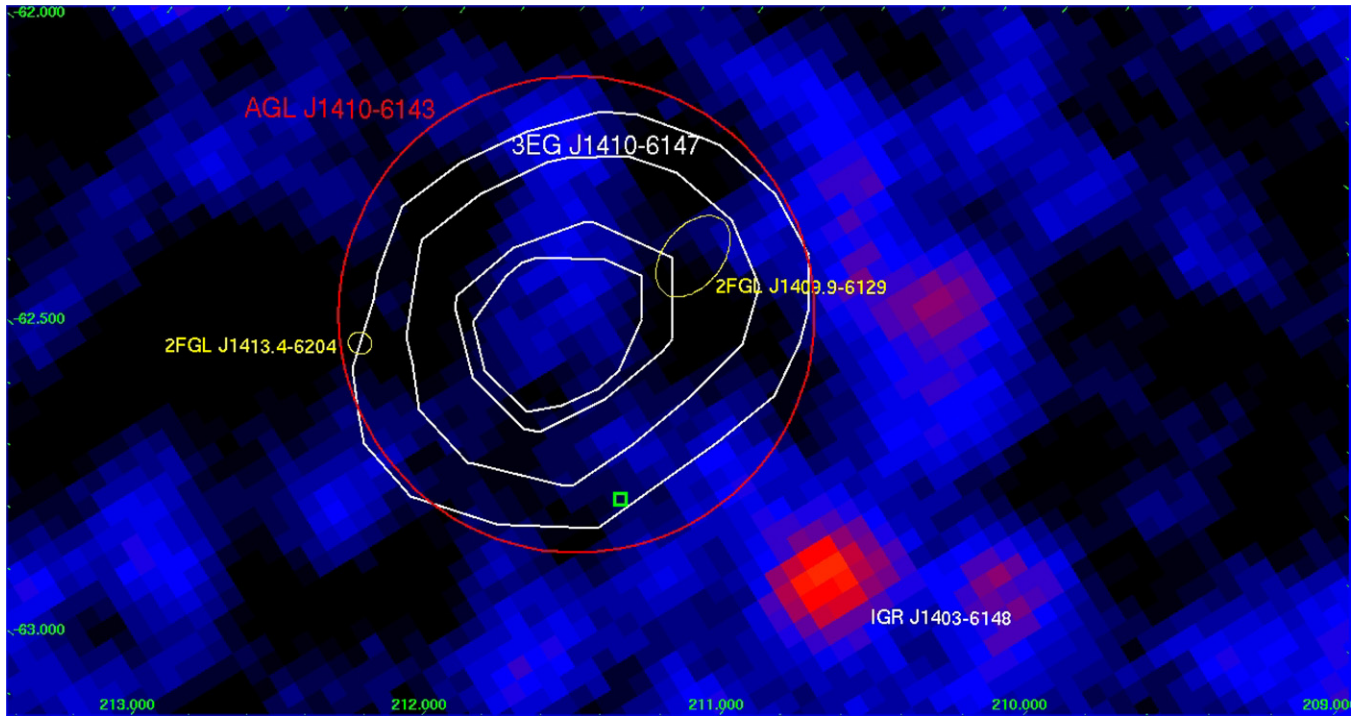


**Figure 7.** Error box of AGL J1410–6143 (big red circle) superimposed on the 20–100 keV *INTEGRAL*/IBIS deep mosaic image ( $\sim 2.3$  ms exposure). The *BeppoSAX*/MECS position of MAXI J1409–619 is marked by the green square. The two small yellow ellipses represent the *Fermi*  $\gamma$ -ray sources 2FGL J1409.9–6129 and 2FGL J1413.4–6204, respectively. White contours (from 50% to 99%) refer to the *EGRET* source 3EG J1410–6147.

(A color version of this figure is available in the online journal.)

$$E_n = m_e c^2 \frac{\sqrt{1 + 2n(B/B_{\text{crit}}) \sin^2 \theta} - 1}{\sin^2 \theta} \frac{1}{1 + z}, \quad (1)$$

where  $m_e$  is the electron rest mass,  $c$  is the speed of light,  $\theta$  is the angle between the photon and the magnetic field direction, and  $B_{\text{crit}} = 4.414 \times 10^{13}$  G is the critical magnetic field strength where the cyclotron energy equals the electron rest mass.

The observed (1:2) and (1:3) ratios of the line energies with respect to the fundamental,  $1.7 \pm 0.2$  and  $2.9 \pm 0.3$ , cannot be explained in terms of Equation (1), as is evident from Figure 6. A fit to the harmonic relation, shown as the dashed line, gives  $E_1 = 41 \pm 3$  keV (in agreement with the best-fit value  $E_{\text{cyc}} = 41 \pm 1$  keV found when imposing the harmonic relation in the spectral fit), but with poor significance ( $\chi^2_{\nu} = 2.27$  for 2 dof). In the same figure we also show the harmonic relation from Equation (1) for different values of the magnetic field and the angle  $\theta$ . Taking into account relativistic effects, we found that the magnetic field responsible for the (1:1) and (1:3) CRFs is about 20% higher than that responsible for the (1:2) CRF.

Two points are worth noticing: it is always the (1:2) resonance that shows the larger disagreement with the harmonic relation, and this could be due to the fact that this CRF is due to pure absorption (Nishimura 2003), while for the other resonances other effects, such as multiple scattering and photon spawning, enter into play (see, e.g., Schönherr et al. 2007, and references therein). Unfortunately, because we are not able to reconstruct the CRF profiles, we cannot extract more information, such as the electron temperature and the geometry of the emitting region.

Second, at variance with the V0332+53 and 4U 0115+63 observations, both performed during giant outbursts, our *BeppoSAX* observations were performed while MAXI J1409–619 was in a low state. This did not allow the study

of the dependence of the CRF parameters as a function of luminosity, an important tool for study of the physical conditions in the line-forming region (Mihara et al. 2004; Nakajima et al. 2006; Klochkov et al. 2011).

The likely early-type optical counterpart and the 500 s pulsation make MAXI J1409–619 an HMXB pulsar. According to the nature of the secondary star we have two possibilities: the source is a supergiant fast X-ray transient (SFXT; Sguera et al. 2005; Negueruela et al. 2006) or a Be/HMXB. In favor of the SFXT interpretation is the highly reddened supergiant as possible counterpart, the typical outburst X-ray luminosity of  $2 \times 10^{37}$  erg s $^{-1}$  (assuming a distance of 14.5 kpc), and the dynamic range of more than two orders of magnitude ( $\sim 300$ ) that is typical of the so-called intermediate SFXT (Sguera et al. 2007; Clark et al. 2010). Against, we have that the source active phase, about two months long (Ueno et al. 2010; Kennea et al. 2011), is significantly longer than that typical of SFXT (see, e.g., Sidoli 2009). If this were the case, then our magnetic field measurement would rule out the magnetar nature for SFXTs (Bozzo et al. 2008). The observed properties of MAXI J1409–619 are also in agreement with those observed in other Be/HMXBs, like 1A 1118–615, a 400 s X-ray pulsar with a hard X-ray spectrum ( $\Gamma \sim 1$ ), a CRF at  $\sim 55$  keV, and long (tens of years) periods of quiescence interrupted by giant (Type-II) outbursts lasting weeks to months in which the X-ray luminosity increases by a factor  $\sim 200$  (see, e.g., Rutledge et al. 2007). This would put the source a factor  $\sim 2$ –3 closer.

Finally, we note that MAXI J1409–619 is located within the 0.5 error box of the unidentified transient MeV source AGL J1410–6143 (see Figure 7) discovered on 2008 February 21 by the  $\gamma$ -ray satellite *AGILE* (Tavani et al. 2009a) during a bright MeV flare lasting only about one day (Pittori et al. 2008; Orlandini et al. 2008). The *AGILE* large



position uncertainty makes it very difficult to identify its lower energy counterpart responsible for the  $\gamma$ -ray emission. Despite this drawback, it is intriguing to note that the flaring source MAXI J1409–619 is the only cataloged hard X-ray source above 20 keV (20–100 keV) to be located inside the *AGILE* error box, according to all the available catalogs in the HEASARC database. This spatial correlation is further supported by a similar transient nature for both MAXI J1409–619 and AGL J1410–6143. We also point out that this is not a unique case. To date, a few HMXBs have been unambiguously detected as flaring MeV sources lasting only a few days (Sabatini et al. 2010; Tavani et al. 2009b; Abdo et al. 2009). In addition, there are several other HMXBs proposed as best candidate counterparts of unidentified transient MeV sources located on the Galactic plane (Sguera et al. 2009, 2011; Sguera 2009). For the sake of completeness, we note that within the large *AGILE* error box there are a number of high-energy MeV sources (see Figure 7): (1) 2FGL J1409.9–6129 and 2FGL J1413.4–6204 have been reported in the second *Fermi* source catalog (Abdo et al. 2012) as firmly identified  $\gamma$ -ray pulsars and this unambiguously excludes their association with the transient AGL J1410–6143 and (2) 3EG J1410–6147 is still unidentified although it has been likely associated with the  $\gamma$ -ray pulsar 2FGL J1409.9–6129 (O’Brien et al. 2008). However, Wallace et al. (2000) reported a possible MeV flare from 3EG J1410–6147 lasting a few days in 1991 November. This behavior is at variance with the proposed association with the  $\gamma$ -ray pulsar 2FGL J1409.9–6129, while it is more compatible with the flaring nature of AGL J1410–6143. Further multi-wavelength studies (radio, NIR, X-ray, and  $\gamma$ -ray) of the sky region are strongly needed and encouraged to shed more light on the nature of such high-energy emitters.

We thank an anonymous referee for helpful comments and suggestions that greatly improved the paper. The *BeppoSAX* satellite was a joint Italian–Dutch program. Part of this work is based on archival data, software or online services provided by the ASI Scientific Data center (ASDC), and the High Energy Astrophysics Science Archive Research Center (HEASARC), provided by NASA’s Goddard Space Flight Center. This publication makes use of data products from the 2MASS archive. The authors acknowledge support from ASI/INAF grants I/088/06/0, I/009/10/0, and I/033/10/0 and grant PRIN INAF/2009.

## APPENDIX A

### ON THE STATISTICAL SIGNIFICANCE OF ABSORPTION FEATURES

The analysis of the significance of spectral absorption features, and in particular CRFs, has historically been fraught with serious misunderstanding that we attribute to the application of techniques made for *emission* features to absorption ones. This has a very profound impact on the statistical analysis, as detailed in the following.

First, when searching for spectral features, and especially absorption features, the binning of data is crucial: indeed a narrow feature can be lost if the data binning is too high (see, e.g., Eadie et al. 1971, page 259), as we showed in the data analysis detailed in Section 2.1.2. But before searching for the best binning factor, it has become customary to rebin data in order to achieve a minimum number of counts in each bin. The reason for this procedure is that we must avoid bins with few counts if we want to use the  $\chi^2$  statistics to test for the goodness of our fit (in other words, errors must be normally distributed).

A minimum 20 counts  $\text{bin}^{-1}$  filter is sufficient to achieve this goal (Cash 1979).

The application of this criterion to background-subtracted spectra is correct for instruments that are not background dominated (that is, they have an intrinsically low number of counts per bin), like a detector on the focal plane of X-ray optics. On the other hand, when the net source spectrum is obtained by subtracting two high counts spectra this correction *must not* be applied (instruments like *BeppoSAX*/PDS or *RXTE*/HEXTE are background dominated, with a very high number of counts per energy channel). Although the net source counts can be very low, they are still Gaussian distributed, because they result from the difference of two normally distributed counts.

Second, if features are present in the source spectrum, they (clearly) show up in the fit residuals, and the standard goodness of fit estimator, the minimization of the  $\chi^2$  statistics (Lampton et al. 1976), should (clearly) indicate that the fit is not “good” and an additional component is necessary. The inclusion of a new component in the continuum should result in a reduction of the reduced  $\chi^2$ . In order to assess whether the improvement of the  $\chi^2$  is due to chance or is because the new component is significant it is customary to use the *F*-test (see, e.g., Barlow 1989, page 160).

A very important point has to be raised here because we have two completely different approaches whether we are dealing with emission or absorption features. In the former case we are dealing, using a XSPEC terminology, with an *additive* component, and we test the null hypothesis that the coefficient of the new term is zero (Bevington 1969, page 200). This is the *F*-test routine that is incorporated in the recent versions of XSPEC.

On the other hand, when dealing with an absorption feature, the component is *not* additive but multiplicative (see routines *gabs* or *cyclabs*). It is therefore obvious that we cannot use the *F*-test for an additive component because we cannot vary to zero the new component coefficient without modifying the parameters of the original model. The two components (the multiplicative model and the original continuum) are strongly coupled and variations in one will affect also the other. Therefore, we must use a different *F*-test, as described in Press et al. (2007, page 730), that tests the null hypothesis that the observed variances come from the same sample (and this routine is *not* incorporated in XSPEC). This same test must be used to assess if two different models are statistically equivalent or not (and indeed we used it in Section 2.1.2 to compare the power-law and the cutoff power-law fits). It is worth noting that the application of the *F*-test to the statistical assessment of CRFs is not affected by the concerns raised by its use with emission lines (Protassov et al. 2002).

Third, CRFs are very shallow features, with their count rates often at the instrument sensitivity level. We therefore expect errors to be dominant, and consequently the  $\chi^2$  could not be the best estimator of the CRF significance. We need a test that takes into account the structure of the line (information which is lost in the  $\chi^2$  because we compute the square of the difference between the data and the model). In other words, we need to compute what is the probability that a particular structure visible in the fit residuals occurs by chance.

The run test (also known as Wald–Wolfowitz test; Barlow 1989; Eadie et al. 1971) works on the *signs* of the deviations, that is, on the form of the residuals. To better clarify how the run test works take a look at Figure 8, adapted from Barlow (1989): when fitting the 12 data points with a straight line the



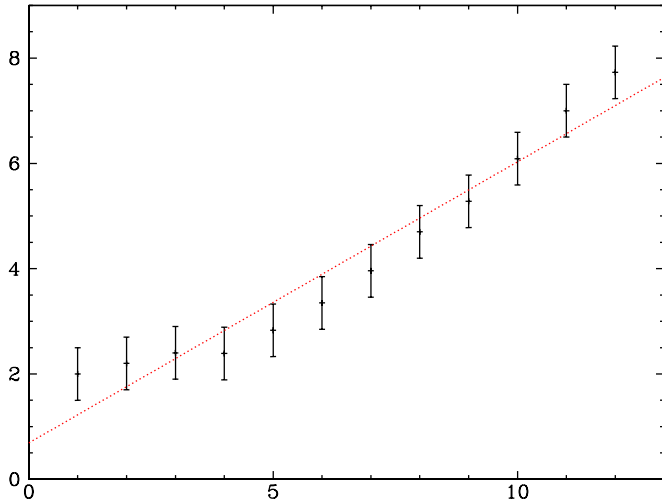


**Figure 8.** Example on how the goodness of fit estimation performed by the  $\chi^2$  statistics not always is able to find the best-fit model to the data. In this case, the linear fit to the 12 data points yields a normalized  $\chi^2$  of 1, but the deviation with respect to the straight line is evident. A run test shows that these deviations have only 1.3% probability to be due to random fluctuations (see the text for details).

(A color version of this figure is available in the online journal.)

normalized  $\chi^2$  is exactly 1 (likely due to error overestimation). But it is evident by eye that the fit is not good (indeed the data come from a parabolic model). The reason is that if the fit were good we should expect that the number of points “above” the fitting line should not group together, but should be intermixed with points “below” the fitting line (and this should be more true as the number of data points increases). If, on the other hand, we observe only small groups of data with the same “sign” (called *runs*), this means that our data are not randomly distributed with respect to the fitting model, but there is an underlying trend.

As we can see from Figure 8, we have 12 points, 6 points “above” the fitting line (let us call them  $N_+$ ) and 6 points “below” the fitting line ( $N_-$ ). The number of runs  $N_r$  is only 3, suspiciously small. Indeed the probability of obtaining  $N_r \leq 3$  is 1.3%, telling us that the structure observed in the residuals is not due to random fluctuations but to a wrong modelization (the linear fit).

From this example, and from the real-case analysis performed on the residuals shown in Figures 5 and 9, it should be clear that the goodness of fit in the case of data structures in the residuals should not be addressed *only* with the  $\chi^2$  estimator, but it has to be supported by the run test.

In conclusion, this is a sort of *cookbook* for a correct evaluation of the statistical significance of absorption (CRFs) features in the spectra of X-ray sources.

1. Be careful with the binning: although CRFs are usually broad features, too small a binning can hide structures. When dealing with background-dominated data (like, for example, *BeppoSAX*/PDS or *RXTE*/HEXTE net spectra), never rebin data in order to have a minimum number of counts per bin, otherwise we risk losing the absorption feature.
2. In order to assess the significance of a CRF the *F*-test is perfectly suitable, but we must use the correct routine: the *F*-test routine included in XSPEC is applicable only to an additive component (in particular, an emission line), while both gabs and cychabs are multiplicative.

**Table 3**  
Best-fit Parameters for the Joint MECS/PDS Spectral Fits

	Power Law	Cutoff	Broken PL	Power Law + 3 gabs
$\Gamma$	$0.87 \pm 0.07$	$-0.75^{+0.3}_{-0.5}$	$0.06^{+0.2}_{-0.2}$	$1.0^{+0.3}_{-0.2}$
$E_{\text{cutoff}}$	...	$14 \pm 4$	$27^{+7}_{-4}$	...
$\Gamma_2$	...	...	$2.93^{+1.9}_{-0.6}$	...
$\chi^2_{\nu}$ (dof)	2.48 (66)	0.91 (65)	0.78 (64)	0.54 (59)

3. The evaluation of the statistical significance of a CRF must be supported by other tests, especially in the presence of structures in the fit residuals: the run test is able to discriminate whether the structure is due to random fluctuations or not.

## APPENDIX B

### THE CONTINUUM SPECTRAL MODEL OF MAXI J1409–619

The analysis performed on the broadband spectrum of the pointed MAXI J1409–619 observation yields as best-fit continuum a power law with index  $\sim 0.9$  (see Section 2.1.1). On the other hand, the analysis performed on a coarser binned spectrum of the offset observation indicates the presence of a change of slope around 20–40 keV (see Section 2.1.2). Because a finer rebinning of this second observation revealed the presence of features that can be explained as CRSFs, it is important to understand whether this change of slope is due to a cutoff in the continuum or is a combined effect of the binning and the presence of the absorption features.

From the pointed observation we know that data below 10 keV must be described by a power law with  $\Gamma \sim 0.9$ . To take into account this constraint we performed a joint fit of the high-energy PDS spectrum from the second observation with the low-energy MECS spectrum from the first observation.

Although the two spectra come from different observations, X-ray pulsars are known to not show any spectral variability besides that at low energy due to reprocessing of X-rays by the circumstellar material (see, for example, the case of Vela X-1 or GX301-2). Because our source does not show any intrinsic absorption or emission lines, signatures of reprocessing, we are confident that our MECS spectrum did not change between the two observations.

First we tried a fit with a power law modified at low energy by photoelectric absorption. All the parameters are left free but the  $N_H$  (fixed at the  $2.8 \times 10^{22} \text{ cm}^{-2}$  value obtained from the ON-source observation), and the result is shown in panel (a) of Figure 9. The fit parameters are listed in Table 3.

The fit is not statistically acceptable, and the slope is driven by the low-energy part of the spectrum. To fit also the PDS data we need something that is able to change the slope at about 40 keV.

Now let us test whether we can explain this change of slope in terms of a cutoff in the continuum. We first tried a cutoff power law (see panel (b) in Figure 9): the fit is statistically acceptable but the power-law index does not match with that of the low-energy part, below 10 keV. The systematic deviations from the model (information lost by the  $\chi^2$  test, as discussed in Appendix A) can be quantified by means of the run test on the MECS residuals ( $N_+ = 8$ ,  $N_- = 6$ , and  $N_r = 3$ ). The probability of obtaining  $N_r \leq 3$  is 0.5%, therefore the structure

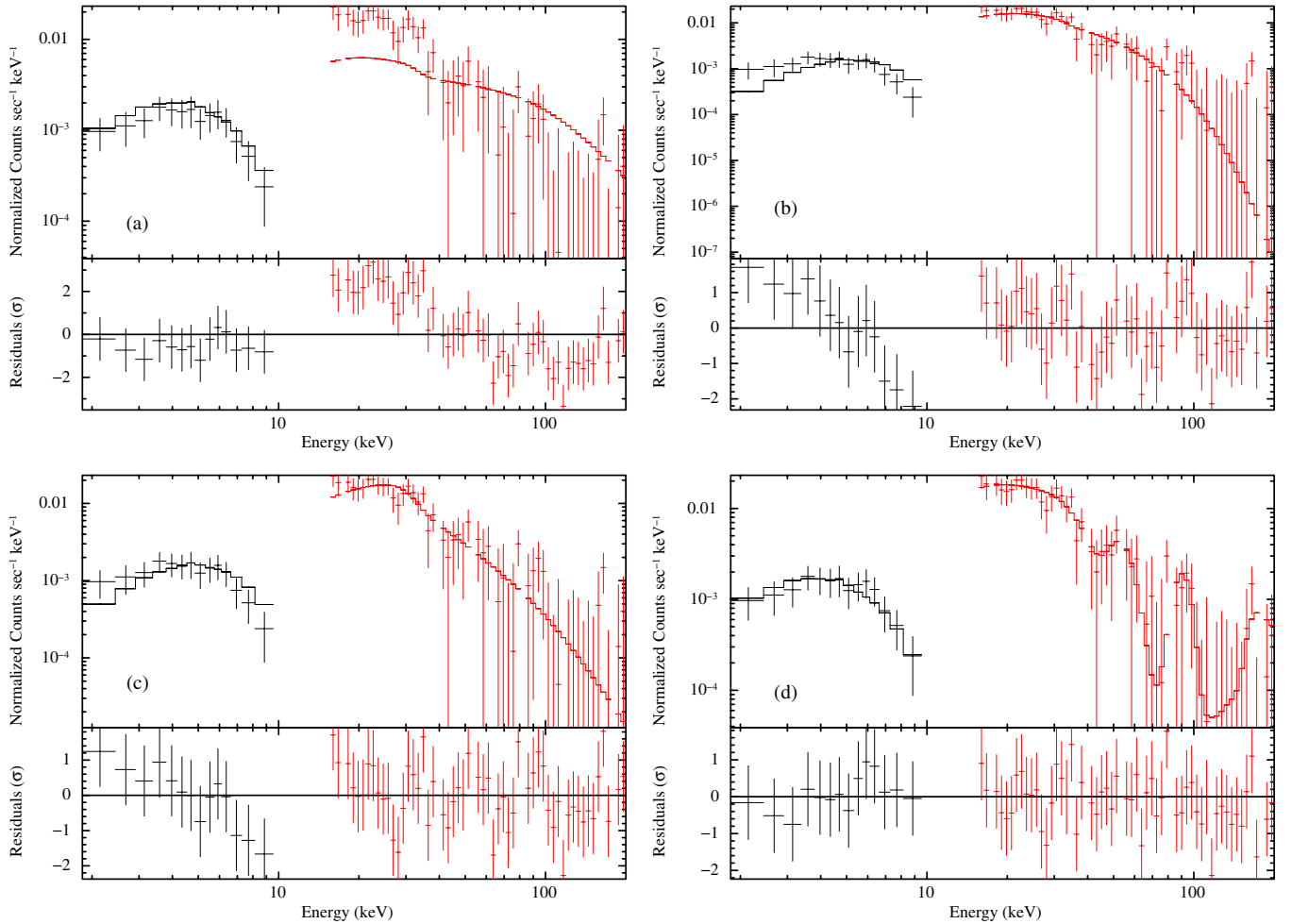


**Figure 9.** 1.8–200 keV joint MECS (from the pointed observation)/PDS (from the offset observation) spectrum. (a) Fit with a power-law continuum. (b) Fit with a cutoff continuum. (c) Fit with a broken power-law continuum. (d) Fit with a power-law continuum and three CRSFs. The only model able to fit simultaneously the low- (below 10 keV) and high-energy data is the power law plus three CRSFs. The best-fit parameters are listed in Table 3.

(A color version of this figure is available in the online journal.)

observed in the residuals is not due to random fluctuations but to the wrong modelization of the continuum. The same result is obtained with the broken power-law fit (see panel (c) in Figure 9): there is no match to the MECS data.

These results demonstrate that the change of slope is not in the continuum but is due to something else: we made the hypothesis that its origin is absorption features. Therefore, the true continuum model is a power law together with CRSF features (see panel (d) in Figure 9). Because we are not able to disentangle the continuum and the CRSFs, due to the breadth of the features and their low statistics, we need to fix the power-law index to the value obtained by the broadband fit.

Just as a test, we performed all the analysis on the CRSFs by fixing the power-law index at 1.0, 1.1, and 1.2, corresponding to the  $1.0 \pm 0.2$  value obtained from the fit to the PDS data below 30 keV and the points trailing the CRSFs. The CRSF parameters are all consistent with each other, demonstrating that they do not depend on the particular value of the power-law index.

## REFERENCES

- Abdo, A. A., Ackermann, M., Ajello, M., et al. 2009, *Science*, **326**, 1512
- Abdo, A. A., Ackermann, M., Ajello, M., et al. 2012, *ApJS*, in press (arXiv:1108.1435)
- Barlow, R. J. 1989, *Statistics: A Guide to the Use of Statistical Methods in the Physical Sciences* (New York: Wiley-Interscience)
- Barthelmy, S. D., Barbier, L. M., Cummings, J. R., et al. 2005, *Space Sci. Rev.*, **120**, 143
- Bevington, P. R. 1969, *Data Reduction and Error Analysis for the Physical Sciences* (New York: McGraw-Hill)
- Bird, A. J., Bazzano, A., Bassani, L., et al. 2010, *ApJS*, **186**, 1
- Boella, G., Butler, R. C., Perola, G. C., et al. 1997a, *A&AS*, **122**, 299
- Boella, G., Chiappetti, L., Conti, G., et al. 1997b, *A&AS*, **122**, 327
- Bozzo, E., Falanga, M., & Stella, L. 2008, *ApJ*, **683**, 1031
- Bradt, H. V., Rothschild, R. E., & Swank, J. H. 1993, *A&AS*, **97**, 355
- Burrows, D. N., Hill, J. E., Nousek, J. A., et al. 2005, *Space Sci. Rev.*, **120**, 165
- Camero-Aranz, A., Finger, M. H., & Jenke, P. 2010, *ATel*, **3069**, 1
- Canuto, V., & Ventura, J. 1977, *Fundam. Cosm. Phys.*, **2**, 203
- Cardelli, J. A., Clayton, G. C., & Mathis, J. S. 1989, *ApJ*, **345**, 245
- Cash, W. 1979, *ApJ*, **228**, 939
- Clark, D. J., Sguera, V., Bird, A. J., et al. 2010, *MNRAS*, **406**, L75
- Coburn, W., Kretschmar, P., Kreykenbohm, I., et al. 2005, *ATel*, **381**, 1
- Cohen, M., & Green, A. J. 2001, *MNRAS*, **325**, 531
- Dickey, J. M., & Lockman, F. J. 1990, *ARA&A*, **28**, 215
- Doherty, M., Johnston, S., Green, A. J., et al. 2003, *MNRAS*, **339**, 1048
- Eadie, W. T., Drijard, D., & James, F. E. 1971, *Statistical Methods in Experimental Physics* (Amsterdam: North-Holland)
- Ferrigno, C., Becker, P. A., Segreto, A., Mineo, T., & Santangelo, A. 2009, *A&A*, **498**, 825
- Frontera, F., Costa, E., dal Fiume, D., et al. 1997, *A&AS*, **122**, 357
- Frontera, F., Orlandini, M., Landi, R., et al. 2007, *ApJ*, **666**, 86
- Gehrels, N., Chincarini, G., Giommi, P., et al. 2004, *ApJ*, **611**, 1005
- Hartman, R. C., Bertsch, D. L., Bloom, S. D., et al. 1999, *ApJS*, **123**, 79
- Heindl, W. A., Coburn, W., Gruber, D. E., et al. 1999, *ApJ*, **521**, L49
- Jahoda, K., Swank, J. H., Giles, A. B., et al. 1996, *Proc. SPIE*, **2808**, 59
- Kennea, J. A., Curran, P., Krimm, H., et al. 2010a, *ATel*, **3060**, 1

- Kennea, J. A., Krimm, H., Romano, P., et al. 2010b, *ATel*, **2962**, 1
- Kennea, J. A., Romano, P., Mangano, V., et al. 2011, in *Proc 4th International MAXI Workshop (Aoyama, Japan)*, to appear (arXiv:1101.6055)
- Klochkov, D., Staubert, R., Santangelo, A., Rothschild, R. E., & Ferrigno, C. 2011, *A&A*, **532**, A126
- Kreykenbohm, I., Mowlavi, N., Produit, N., et al. 2005, *A&A*, **433**, L45
- Lampton, M., Margon, B., & Bowyer, S. 1976, *ApJ*, **208**, 177
- Lang, K. R. 1992, *Astrophysical Data: Planets and Stars* (New York: Springer)
- Masetti, N., Parisi, P., Palazzi, E., et al. 2010, *A&A*, **519**, A96
- Matsuoka, M., Kawasaki, K., Ueno, S., et al. 2009, *PASJ*, **61**, 999
- Meegan, C., Bhat, N., Connaughton, V., et al. 2007, in *AIP Conf. Ser.* 921, *The First GLAST Symposium*, ed. S. Ritz, P. Michelson, & C. A. Meegan (Melville, NY: AIP), 13
- Meszáros, P. 1992, *High Energy Radiation from Magnetized Neutron Stars* (Chicago: Univ. Chicago Press)
- Mihara, T., Kawai, N., Yoshida, A., et al. 2002, *Proc. SPIE*, **4497**, 173
- Mihara, T., Makishima, K., & Nagase, F. 2004, *ApJ*, **610**, 390
- Monet, D. G., Levine, S. E., Canzian, B., et al. 2003, *AJ*, **125**, 984
- Nakajima, M., Mihara, T., Makishima, K., & Niko, H. 2006, *ApJ*, **646**, 1125
- Negueruela, I., Smith, D. M., Reig, P., Chaty, S., & Torrejón, J. M. 2006, in *Proc. The X-ray Universe 2005*, ed. A. Wilson (ESA Special Publication, Vol. 604), 165
- Nishimura, O. 2003, *PASJ*, **55**, 849
- Nishimura, O. 2005, *PASJ*, **57**, 769
- Nishimura, O. 2008, *ApJ*, **672**, 1127
- O'Brien, J. T., Johnston, S., Kramer, M., et al. 2008, *MNRAS*, **388**, L1
- Orlandini, M. 2004, in *X-ray and Gamma-ray Astrophysics of Galactic Sources*, 4th AGILE Science Workshop, ed. M. Tavani, A. Pellizoni, & S. Vercellone (Rome: Aracne Editrice) (arXiv:astro-ph/0402628), 119
- Orlandini, M., dal Fiume, D., Frontera, F., et al. 1998, *ApJ*, **500**, L163
- Orlandini, M., Frontera, F., Bassani, L., Landi, R., & Sguera, V. 2008, *ATel*, **1419**, 1
- Parmar, A. N., Martin, D. D. E., Bavdaz, M., et al. 1997, *A&AS*, **122**, 309
- Perri, M., & Capalbi, M. 2002, *A&A*, **396**, 753
- Pittori, C., Verrecchia, F., Santolamazza, P., et al. 2008, *ATel*, **1394**, 1
- Predehl, P., & Schmitt, J. H. M. M. 1995, *A&A*, **293**, 889
- Press, W. H., Teukolsky, S. A., Vetterling, W. T., & Flannery, B. P. 2007, *Numerical Recipes: The Art of Scientific Computing* (Cambridge: Cambridge Univ. Press)
- Protassov, R., van Dyk, D. A., Connors, A., Kashyap, V. L., & Siemiginowska, A. 2002, *ApJ*, **571**, 545
- Rutledge, R. E., Bildsten, L., Brown, E. F., et al. 2007, *ApJ*, **658**, 514
- Sabatini, S., Tavani, M., Striani, E., et al. 2010, *ApJ*, **712**, L10
- Santangelo, A., Segreto, A., Giarrusso, S., et al. 1999, *ApJ*, **523**, L85
- Schönherr, G., Wilms, J., Kretschmar, P., et al. 2007, *A&A*, **472**, 353
- Sguera, V. 2009, in *7th INTEGRAL Workshop: An INTEGRAL View of Compact Objects*, PoS(Integral08)082 (arXiv:0902.0245)
- Sguera, V., Barlow, E. J., Bird, A. J., et al. 2005, *A&A*, **444**, 221
- Sguera, V., Drave, S. P., Bird, A. J., et al. 2011, *MNRAS*, **417**, 573
- Sguera, V., Hill, A. B., Bird, A. J., et al. 2007, *A&A*, **467**, 249
- Sguera, V., Orlandini, M., Frontera, F., Bazzano, A., & Bird, A. J. 2010, *ATel*, **2965**, 1
- Sguera, V., Romero, G. E., Bazzano, A., et al. 2009, *ApJ*, **697**, 1194
- Sidoli, L. 2009, *Adv. Space Res.*, **43**, 1464
- Skrutskie, M. F., Cutri, R. M., Stiening, R., et al. 2006, *AJ*, **131**, 1163
- Tavani, M., Barbiellini, G., Argan, A., et al. 2009a, *A&A*, **502**, 995
- Tavani, M., Bulgarelli, A., Piano, G., et al. 2009b, *Nature*, **462**, 620
- Tsygankov, S. S., Lutovinov, A. A., Churazov, E. M., & Sunyaev, R. A. 2006, *MNRAS*, **371**, 19
- Ueno, S., Sugizaki, M., Negoro, H., et al. 2010, *ATel*, **3067**, 1
- Wallace, P. M., Griffiths, N. J., Bertsch, D. L., et al. 2000, *ApJ*, **540**, 184
- Wegner, W. 1994, *MNRAS*, **270**, 229
- Yamamoto, T., Nakajima, M., Yamaoka, K., et al. 2010, *ATel*, **3070**, 1
- Yamaoka, K., Kaaret, P., Nakahira, S., et al. 2010a, *ATel*, **2969**, 1
- Yamaoka, K., Nakahira, S., Negoro, H., et al. 2010b, *ATel*, **2959**, 1